

Investigation of Frequency Characteristics in Cutting of Soft Tissue Using Prototype Ultrasonic Knives

Kosuke EBINA, Hideyuki HASEGAWA, and Hiroshi KANAI*

Graduate School of Engineering, Tohoku University, Sendai 980-8579, Japan

(Received November 24, 2006; revised March 21, 2007; accepted April 5, 2007; published online July 26, 2007)

Recently, ultrasonic surgical knives have been applied in a variety of surgical operations. In this paper, the operation frequency of a surgical knife is focused on. Prototype ultrasonic knives operated at 24.3, 44.3, and 71.9 kHz were constructed. Differences in the effects on soft tissue depending on the operation frequency were investigated using these knives. Frequency characteristics were measured using two parameters: *coagulation ratio* and *coagulated depth*. For the same vibration velocity, at a lower frequency, the distribution of the coagulated tissue was deep and in a narrower region around the center of the tip. For the same vibration amplitude, the coagulated depth at each frequency was similar for all these frequencies. Furthermore, the dependences of tissue coagulation on the vibration velocity, pressure load, contact of the tip with tissue, and direction of vibration were investigated. From these investigations, it was found that the mechanical effect, rather than ultrasound absorption, is the dominant factor in tissue coagulation. [DOI: 10.1143/JJAP.46.4793]

KEYWORDS: ultrasonic surgical knife, frequency characteristic, coagulation ratio, coagulated depth, heat generation, stress-strain relationship

1. Introduction

Recently, there are many studies on the medical treatment technology using ultrasound in addition to those on the development of ultrasonic-diagnosis technology. For instance, focused ultrasound has been applied in extracorporeal shock wave lithotripsy^{1–5)} and controlled ultrasound pulses are expected to be used for making a perforation in the atrial septum.^{6,7)} In this paper, we focus on an ultrasonic surgical knife, which is one of the medical treatment technologies using ultrasound.^{8,9)} It works in the frequency range from 20 to 100 kHz and it fragments tissues by means of various effects, such as mechanical, cavitation, and thermal effects. It is able to cut soft tissue using ultrasonic vibrations of the blade and at the same time, stop bleeding by coagulation. Moreover, it can coagulate proteins at a comparatively low temperature, resulting in less injury, which is a great advantage in surgery. Thus, the existing ultrasonic surgical knife (Johnson & Johnson, Harmonic Scalpel[®], operating frequency = 55.5 kHz) has been applied in a variety of surgical operations, e.g., cutting lung parenchyma,¹⁰⁾ latissimus dorsi muscle mobilization,¹¹⁾ redo cardiac surgery,¹²⁾ thyroidectomy,¹³⁾ tonsillectomy,¹⁴⁾ and harvesting of arterial conduits in coronary artery bypass.¹⁵⁾ These studies show that the use of the Harmonic Scalpel leads to less bleeding, reduction of complications and shortening of operation time compared with conventional techniques using other mechanical surgical knives such as an electrocautery scalpel. Ultrasonic surgical knives of several operating frequencies are available (e.g., Johnson & Johnson, Harmonic Scalpel[®]: 55.5 kHz; Autosuture, Auto-Sonix[™]: 55.5 kHz; Olympus, SonoSurg: 23.5/47 kHz; Aloka, SONOP 5000: 23/35 kHz), however, the effects of the vibration frequency on cutting have not been thoroughly investigated. In recent work, some important parameters, that affect tissue fragmentation, including the operation frequency of the knife and stroke amplitude of the tip, have been studied.¹⁶⁾ Furthermore, the temperature elevation in tissue during operation has been examined,¹⁷⁾ and the acoustic output of the Harmonic Scalpel has been designated

for safe use.¹⁸⁾ Moreover, the influence of various tissue types on the working characteristics of the Harmonic Scalpel has been studied in order to increase its efficiency.¹⁹⁾ However, the effects of the ultrasound vibration of the blade, particularly the effects on the tissue caused by the vibration of the knife tip have not yet been revealed thoroughly. In this paper, we focus on the operating frequency of an ultrasonic surgical knife. The objective of this study is to investigate the frequency characteristics in the cutting of soft tissue using prototype knives operated at several different frequencies (e.g., 20 and 40 kHz and higher) to identify the optimum operation frequency of the ultrasonic surgical knife. As the first stage of this investigation, prototype ultrasonic knives were constructed using bolt-clamped Langevin-type transducers (BLTs) at operation frequencies of 20, 39, and 60 kHz. Then, soft tissue was coagulated with the developed knives, and the frequency characteristics in the cutting of soft tissue were evaluated using two parameters. Furthermore, these results are discussed in terms of the heat generation caused by the stress-strain relationship and ultrasound absorption in soft tissue.

2. Structures of Prototype Knives

Figure 1 shows the technical drawings of the prototype knives. These knives were constructed using BLTs operated at frequencies of 20, 39, and 60 kHz (Honda Electronics, HEC-3020P2B, HEC-3039P4B, HEC-1560P4B, respectively). The structure of the vibration amplifier was a two-stage horn and it was made from duralumin. The stepped horn, which can yield a higher transmutation ratio compared with other shapes, was selected. The theoretical transmutation ratios of these horns were 3.5 and 9.1. The flange, which was 2–4 mm in thickness, was equipped to clamp the knife at the ultrasonic vibration node. The lengths of the knives including transducers were 338, 176, and 113 mm corresponding to 1.5 times the ultrasonic wavelength at the respective frequencies. Moreover, the prototype knives shown in Fig. 1 were used to evaluate tissue coagulation. Thus, these shapes and configurations are different from those of existing ultrasonic surgical knives. Furthermore, impedance matching will be effective in increasing the vibration velocity. Thus, an electric transformer was

*E-mail address: hkanai@ecei.tohoku.ac.jp

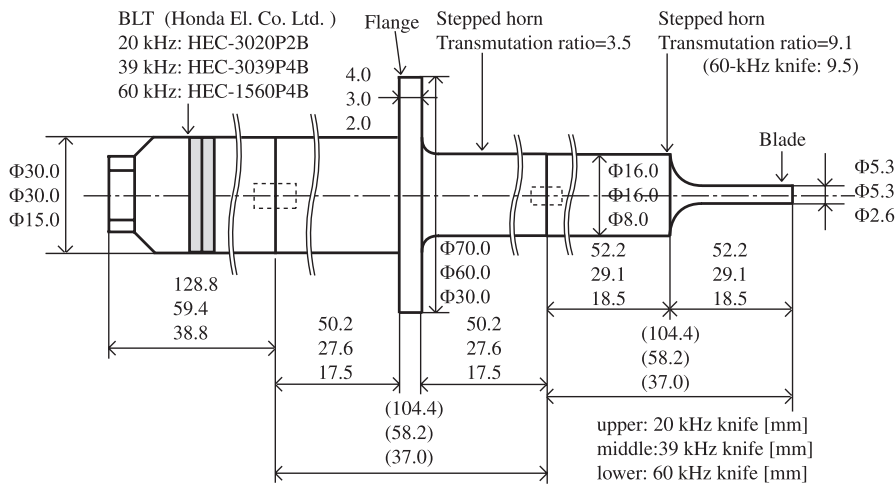


Fig. 1. Technical drawing of the prototype knife.

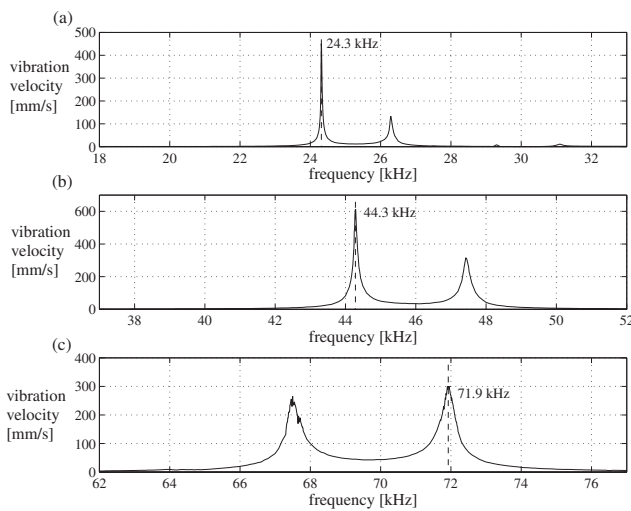


Fig. 2. Frequency response of vibration velocity of the tip of the knife.

mounted between the power amplifier and the knife for impedance matching.

Figure 2 shows the frequency responses of vibration velocities for all knives. Vibration velocities shown in Fig. 2 are peak-to-zero values. From Fig. 2, the maximum vibration velocities were obtained at 24.3, 44.3, and 71.9 kHz for these knives. Thus, these frequencies were employed when the knives were applied to a tissue phantom.

3. Experimental Procedure

Figure 3 shows the experimental setup used in this study. A developed knife was clamped at the flange. In this study, chicken muscle was used. A laser Doppler vibrometer (LDV; Ono Sokki, LV-1300) was used to measure the vibration velocity of the tip of the knife. The laser head was fixed at angle θ relative to ultrasound propagation. The tilted laser ray was incident at a point 5 mm from the tip of the knife. A retroreflective tape reflector, which reflects rays along their incident direction, was attached near the tip of the blade. It was confirmed that there is no change in the condition of the tape reflector, such as detachment, after driving the knife at a velocity of 4 m/s (peak-to-zero). The laser ray must be perpendicular ($\theta = 180^\circ$) to the measurement site in order to measure the correct vibration velocity.

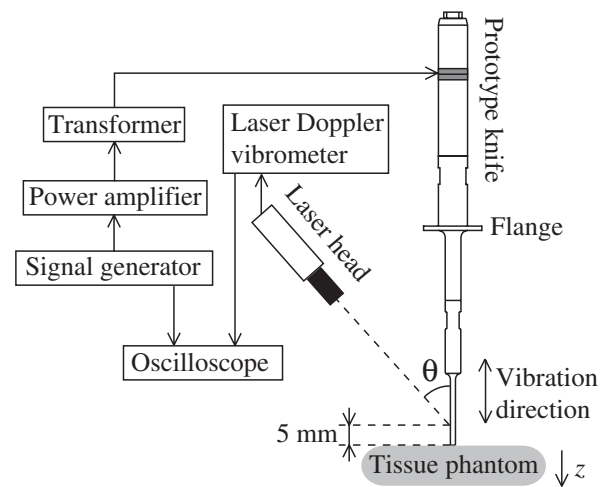


Fig. 3. Experimental setup for measurement of frequency characteristic.

However, it is difficult to keep the laser ray perpendicular to the tip in this setup because the tip was in contact with the tissue phantom. Moreover, near the tip of the knife, tissue fragments and water mist on the surface give rise to undesired effects on the laser ray during the operation, decreasing the laser reflection intensity. Therefore, before the setting of tissue, the LDV was calibrated by analyzing two signals from perpendicular to the tip of the knife ($\theta = 180^\circ$) and from the angle θ . As a result, the vibration velocity was quantitatively defined. The angle θ was set to 37, 43, and 43° for the knives at the driving frequencies of 24.3, 44.3, and 71.2 kHz, respectively.

The coagulation test is described as follows. First, each prototype knife was operated and tissue was coagulated by the vibration at the tip of the knife. Then, the coagulated tissue was cut at the center of the area of tip contact using a surgeon's knife to obtain a cross-sectional image. This image was used to measure the coagulated depth to evaluate the coagulation along the z direction. The coagulation ratio was defined as the area of the coagulated region divided by that of the surface of the tip. It was used for the evaluation of the coagulation on the surface of the tissue. These two parameters were used in the investigation of the frequency characteristics in the cutting of soft tissue. These procedures were repeated eight times for each knife.

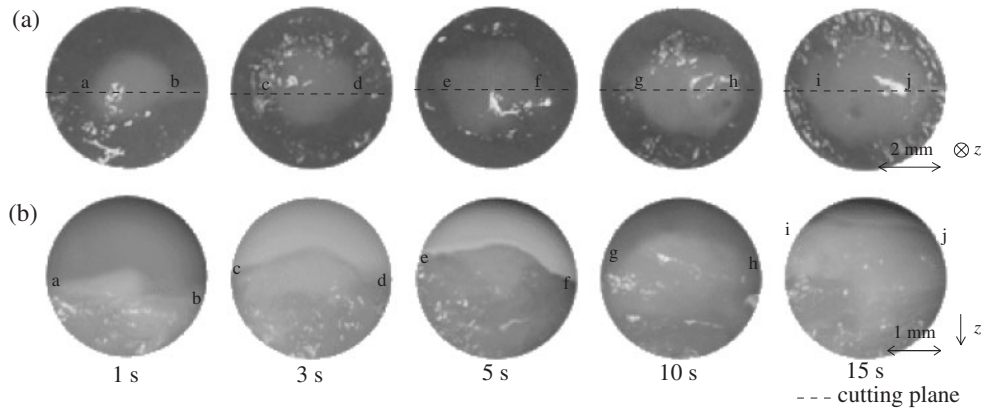


Fig. 4. Results of the cutting test using the 20 kHz knife. (a) Tissue surface after the cutting test. (b) Magnified cross-sectional views along broken lines in (a).

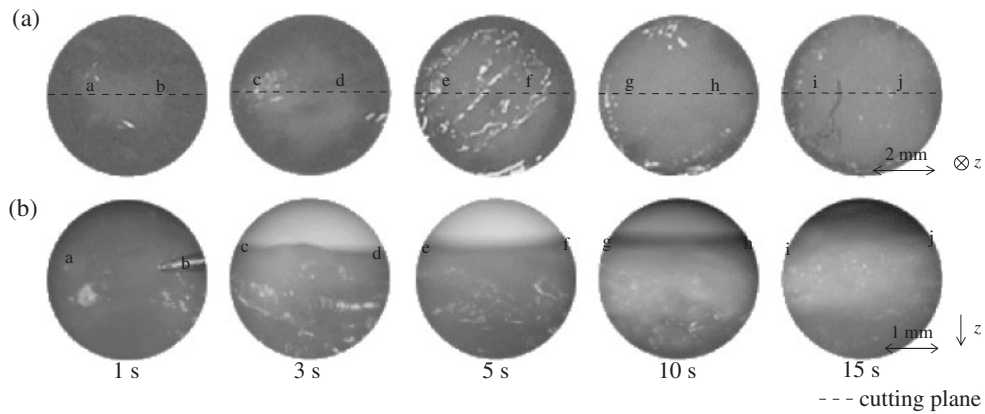


Fig. 5. Results of the cutting test using the 40-kHz knife. (a) Tissue surface after the cutting test. (b) Magnified cross-sectional views along broken lines in (a).

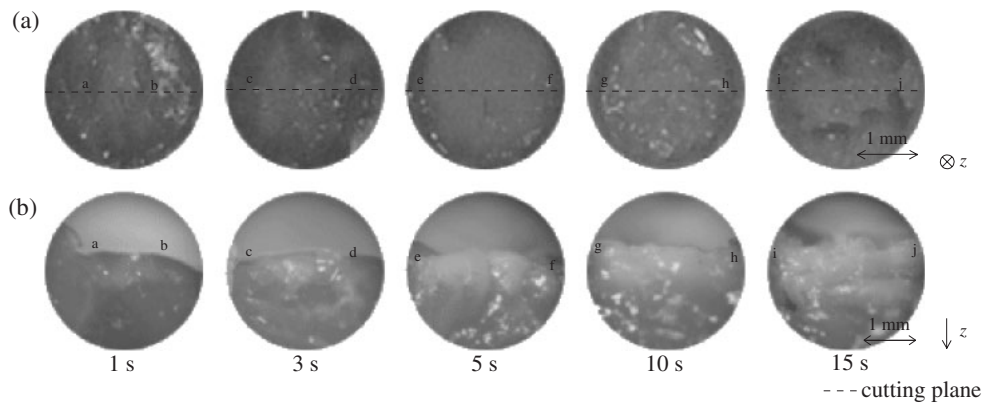


Fig. 6. Results of the cutting test using the 60-kHz knife. (a) Tissue surface after the cutting test. (b) Cross-sectional views along broken lines in (a).

4. Results

4.1 Results of tissue coagulation test

First, the vibration velocity was set to 2.0 m/s for all knives. In this experiment, the prototype knives were operated at 24.2, 44.8, and 71.4 kHz. The peak-to-zero value of the vibration velocity is shown in all figures in this paper. The tip was brought into contact with the soft tissue for 1, 3, 5, 10, and 15 s with or without load.

Figure 4 shows the coagulated tissue sample for various operating periods using the 20 kHz knife. The images of the

coagulated tissue using the 40 kHz knife and the 60 kHz knife are shown in Figs. 5 and 6, respectively. In Figs. 4(a), 5(a), and 6(a), the area of the circle is equivalent to that of the tip of a knife. The broken lines in Figs. 4(a), 5(a), and 6(a) show the positions of cutting planes of the cross-sectional images shown in Figs. 4(b), 5(b), and 6(b). In Figs. 4(a), 5(a), and 6(a), the positions of the letters (from a to j) correspond to those in Figs. 4(b), 5(b), and 6(b). In each of Figs. 4(a), 5(a), and 6(a), the coagulation on the surface of tissue spread from the central part to the entire region of tip contact. Moreover, the tissue was coagulated more deeply as

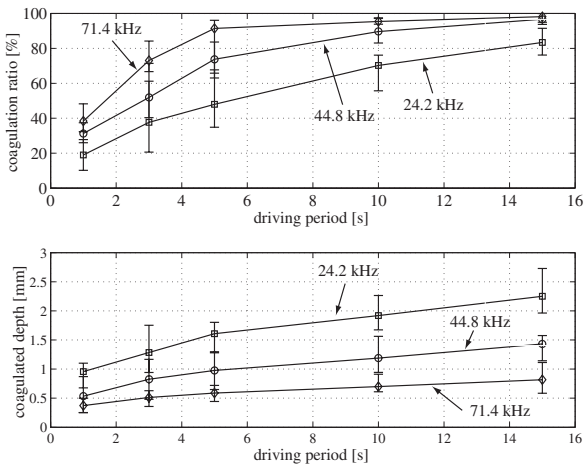


Fig. 7. (a) Measured coagulation ratio. (b) Measured coagulated depth.

the contact time increased as shown in Figs. 4(b), 5(b), and 6(b). These tendencies were similar for the three different frequencies.

Figure 7 shows the measured coagulation ratio and coagulated depth for various driving periods as the mean and ranges (minimum and maximum) of eight measurements. In Fig. 7(a), the coagulation ratio became larger as the driving period increased, as evident in the images in Figs. 4(a), 5(a), and 6(a). The coagulation ratio at a higher frequency tends to be larger than that at a lower frequency. That is, at a lower frequency, coagulation on the surface is slow compared with that at a higher frequency. On the other hand, Fig. 7(b) indicates that the tissue was coagulated more deeply at a lower frequency than at a higher frequency. At 44.8 and 71.4 kHz, the average coagulation ratio at 15 s approached 100%, as shown in Figs. 5(a) and 6(a). These results show that coagulation on the soft tissue approaches saturation.

Next, the relationship between tissue coagulation and the output of the knife, such as amplitude of vibration velocity and displacement, was investigated using the same system that illustrated in Fig. 3. In this measurement, the vibration velocity was changed from 0.6 to 2.0 m/s (peak-to-zero). The prototype knives were operated at 24.3, 44.3, and 71.7 kHz. Figures 8 and 9 respectively show the measured coagulation ratio and coagulated depth obtained after a 10-s drive for various vibration amplitudes, velocities, accelerations, and ultrasound intensities as mean and ranges (minimum and maximum) of eight measurements. The ultrasound intensity I was calculated as $I = (1/2) \cdot \rho c v^2$ (v : vibration velocity, ρ : density = 1,055 kg/m³, c : sound speed = 1,575 m/s²⁰). In Figs. 8 and 9, both the coagulation ratio and coagulated depth increased as the output of the knife increased. In addition, the change in the coagulation ratio among the driving frequencies in Fig. 8(b) was smaller than those in Figs. 8(a) and 8(c). That is, the coagulation on the tissue surface depends on the vibration velocity.

As shown in Fig. 9(a), when the vibration amplitude is smaller than 5 μ m (peak-to-zero), the tissue coagulation along the z axis (depth) is proportional to the vibration amplitude, and does not depend on the vibration frequency.

Figure 10 shows the coagulation ratio in Fig. 8(a) and the coagulated depth in Fig. 9(a) for three operation frequencies,

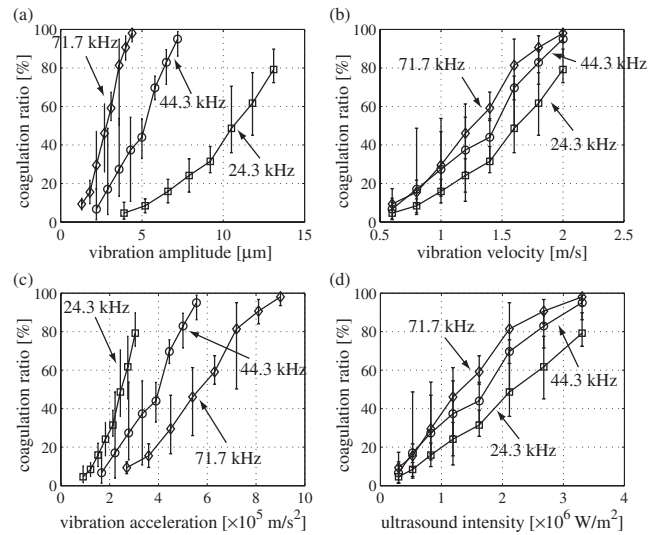


Fig. 8. Measured coagulation ratio versus (a) vibration amplitude, (b) vibration velocity, (c) vibration acceleration, and (d) ultrasound intensity.

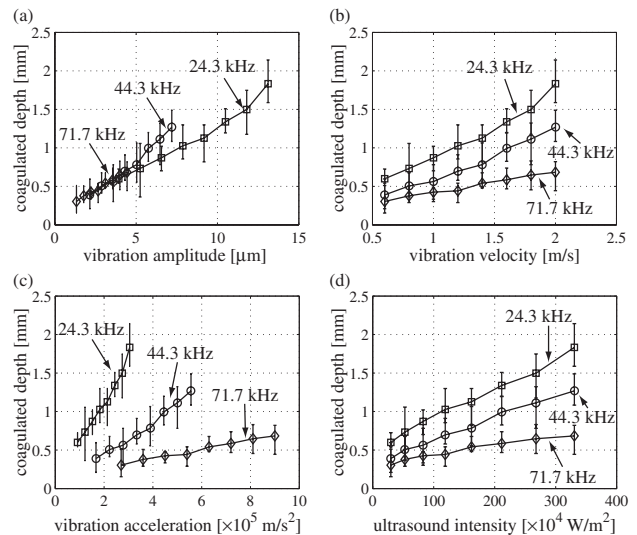


Fig. 9. Measured coagulated depth versus (a) vibration amplitude, (b) vibration velocity, (c) vibration acceleration, and (d) ultrasound intensity.

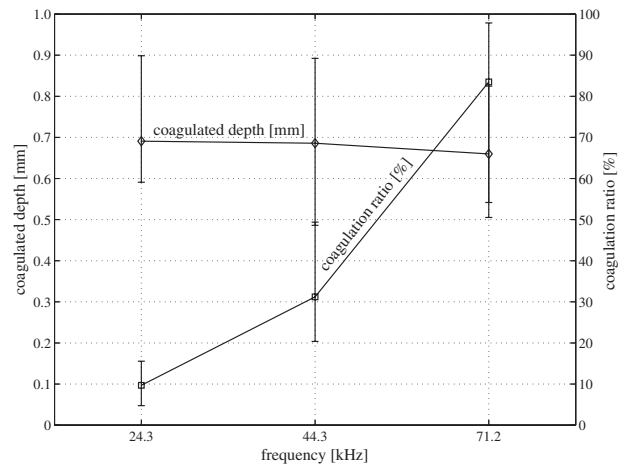


Fig. 10. Results of measuring the coagulation ratio and the coagulated depth at a constant vibration amplitude (4 μ m) for each operation frequency.

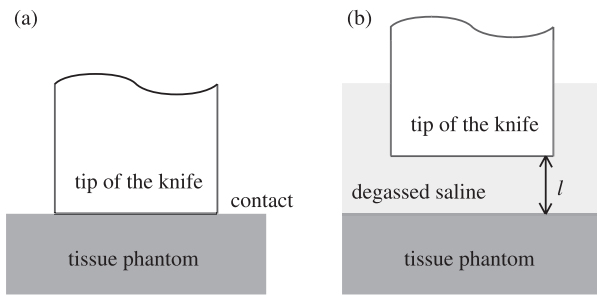


Fig. 11. Experimental setup. (a) Tip of the knife was kept contact with the surface. (b) Tip of the knife was separated from the tissue surface.

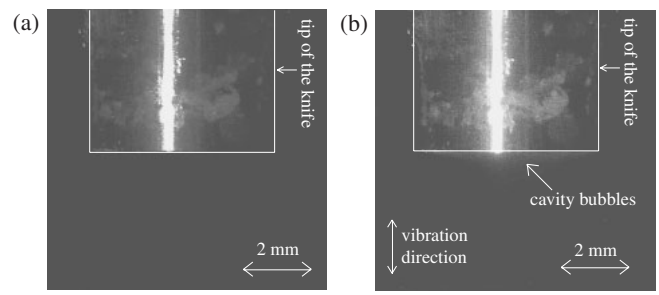


Fig. 13. Magnified view of the tip of the knife. (a) Before operation. (b) During operation.

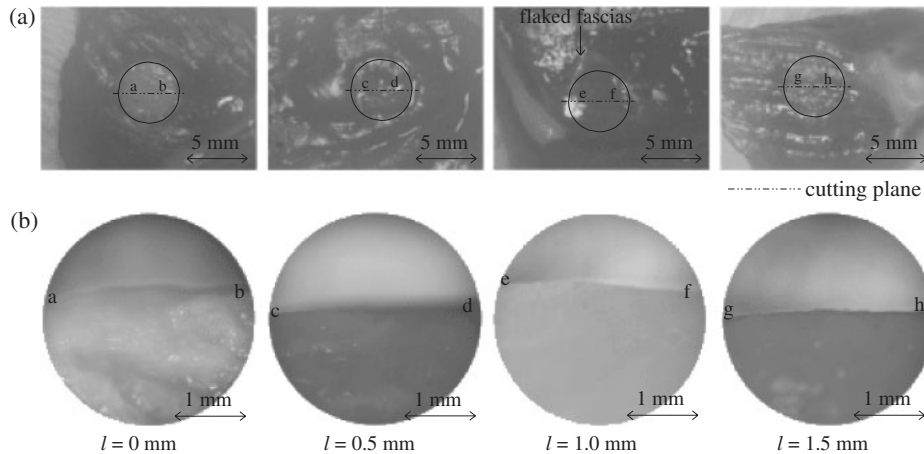


Fig. 12. Coagulated tissue in degassed saline. (a) Tissue surface. (b) Cross-sectional views of (a).

where the vibration amplitude and the driving period were $4\mu\text{m}$ and 10 s, respectively. The coagulated depth did not change for various operation frequencies. However, the coagulation ratio became larger with frequency because the vibration velocity increased with frequency.

4.2 Identification of dominant effect in tissue coagulation

Effects on the tissue caused by the vibration at the tip of the knife is divided into the following two phenomena. The first is the mechanical effect due to tissue expansion and contraction caused by the tip vibration. The second is the acoustic effect caused by the exposure to strong ultrasound and resulting in the cavitation and ultrasound absorption. The absorption coefficient of ultrasound absorption is roughly 0.07 dB/cm at the frequency of 1 MHz in tissue. That is, half the energy of the ultrasound is converted to heat when 1-MHz-frequency ultrasound propagates for 5 cm.²¹⁾ In addition, the absorption coefficient is proportional to the square of the ultrasound frequency, and it is roughly estimated to be 2.52×10^{-4} dB/cm at 60 kHz. Thus, it is very small within the frequency range employed in this study. That is, the temperature elevation due to ultrasound absorption is small. Thus, under the conditions adopted in this study, the acoustical effect on tissue coagulation is limited to the cavitation phenomenon.

In order to investigate the above phenomena, the soft tissue was coagulated in a water bath filled with degassed saline, and the distance l from the tip of the knife to the tissue surface was changed from 0 to 1.5 mm, as shown in Fig. 11. When the distance l is larger than 0 mm, the direct mechanical effect does not affect the tissue and tissue is

coagulated by the cavitation phenomenon. The vibration velocity was set to 2 m/s (peak-to-zero), the driving period was 10 s, and the driving frequency was 44.3 kHz.

The solid circles in Fig. 12(a) show the positions of the tip of the knife. Each line segment in Fig. 12(a) corresponds to that in Fig. 12(b). When the tip of the knife was brought into contact with the tissue surface ($l = 0$ mm), the coagulated tissue (white part) became visible, as shown in Fig. 12. However, when the tip of the knife was separated from the tissue ($l = 0.5$ mm or more), tissue was not coagulated. When $l = 0.5, 1,$ or 1.5 mm, a slight abruptness of the tissue surface was alternatively observed.

Figure 13 shows the magnified view of the driving tip of the knife in water. In Fig. 13(b), cavity bubbles appear as a white haze that is distributed in the region within 0.9 mm from the tip. Thus, damages on the tissue surface would be caused by shock waves due to the breakdown of cavity bubbles. Although such acoustical effect contributes somewhat to the coagulation of the tissue, it is not a major factor in tissue coagulation in Fig. 12 ($l = 0$ mm).

4.3 Relationship between static load and tissue coagulation

The coagulation ratio and coagulated depth were measured for various values (from 0 to 89 kPa) of the static pressure of the contact of the tip with tissue. The vibration velocity and driving period were set at 2 m/s (peak-to-zero) and 5 s, respectively. The driving frequencies of the knives were 24.2, 44.8, and 71.5 kHz. Figure 14 shows the experimental results. In Fig. 14, the coagulation ratio and the coagulated depth became larger for all frequencies as the pressure in-

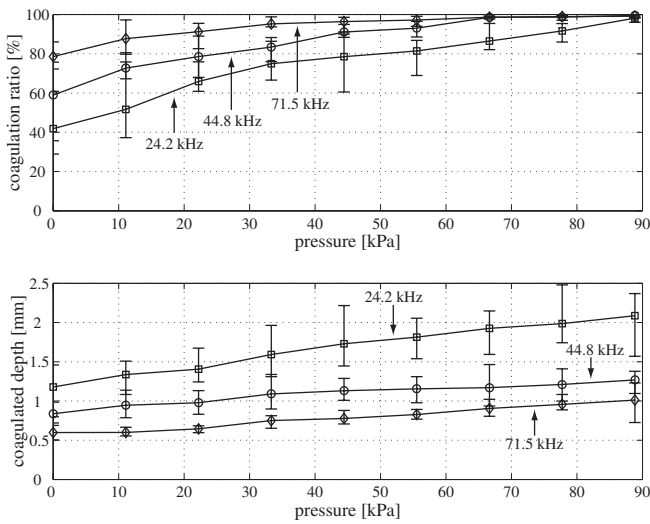


Fig. 14. Relationship between load and tissue coagulation. (a) Coagulation ratio. (b) Coagulated depth.

creased. In the experiments described above, the tip of the knife was in contact with the tissue surface without load. When the load was applied, it compressed the tissue, and mechanical viscoelastic properties were changed by the pressure. However, the cavitation phenomenon, which is an acoustical effect, depends not on the applied pressure but on the ultrasound intensity. On the other hand, the heat generation caused by expansion and contraction of tissue in the mechanical effect depends on the viscoelasticity. This result shows that the heat generation increases with pressure force.

4.4 Comparison of tissue coagulation due to the difference in vibration direction

Figure 12 shows that the mechanical effect due to the vibration of the knife tip is a dominant factor in soft tissue coagulation. The tissue coagulation due to the mechanical effect is caused by thermal denaturation due to heat generation. Heat generation is divided into the following two phenomena: frictional heat at the interface between the knife and the soft tissue and heat generation caused by expansion and contraction of the tissue. To investigate the difference between these two types of heat generations, the tip (edge or side) was brought into contact with tissue in the two manners as shown in Figs. 15(a) and 15(b). Heat will be

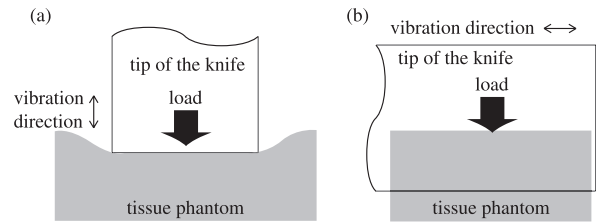


Fig. 15. Experimental setup for investigating the tissue coagulation depending on vibration direction. (a) Longitudinal direction. (b) Lateral direction.

generated by longitudinal strain in the case of Fig. 15(a) and by shear strain or friction in the case of Fig. 15(b). This experiment was carried out using the 39 kHz knife at a driving frequency of 44.3 kHz.

Figure 16 shows the difference in the coagulated tissues. In Fig. 16(c), the points marked by letters (from a to d) correspond to those in Fig. 16(d). In Fig. 16(a), for the vibration velocity of 2 m/s, the tissue was seen to be coagulated by the longitudinal vibration but not by the lateral vibration. Since the frictional force is proportional to the normal pressure, the tissue load was increased from 100 to 400 g. However, tissue was not coagulated even with the load of 400 g, as shown in Fig. 16(b). On the other hand, when using the vibration velocity of 4 m/s, as shown in Fig. 16(c), the tissue phantom was coagulated for both cases of the vibration direction. However, as seen from the cross-sectional view in Fig. 16(d), the depth of the coagulated regions due to longitudinal and lateral vibrations were 2.67 and 0.67 mm, respectively. Heat generation by longitudinal strain was larger than those by shear strain and frictional heat. Therefore, tissue coagulation is mainly caused by heat generation due to longitudinal strain.

5. Discussion

In this study, since coagulation did not occur when the tip of the knife was separated from tissue, tissue coagulation was caused not by ultrasound absorption but by heat generation due to the deformation of tissue. Therefore, the coagulation resulting from heat generation is considered to occur via the deformation of tissue. The viscoelasticity of tissue is approximated using the Voigt model, as shown in Fig. 17. The basic equation of the Voigt model is given by

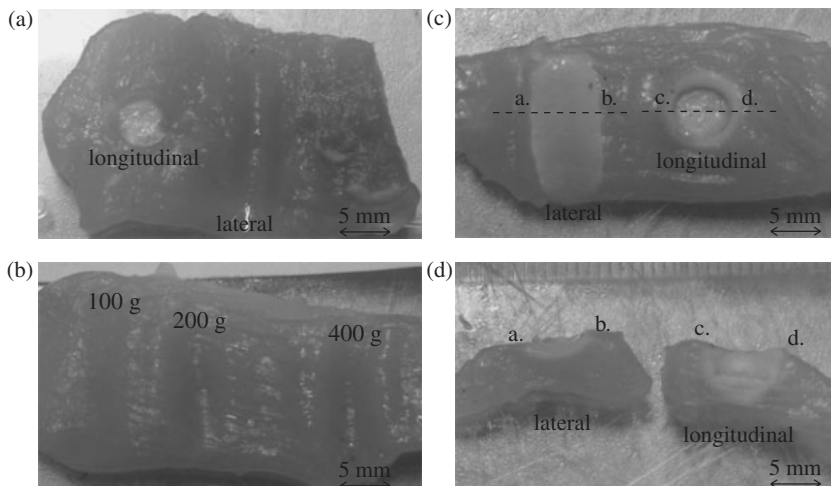


Fig. 16. Difference in tissue coagulation depending on (a) vibration direction (vibration velocity = 2 m/s, load = 200 g, driving period = 10 s), (b) pressure load (lateral vibration, vibration velocity = 2 m/s, driving period = 20 s, tissue load = 100 g (left), 200 g (center), and 400 g (right)), and (c) vibration direction (vibration velocity = 4 m/s, load = 200 g, driving period = 10 s). (d) Cross-sectional view of (c).

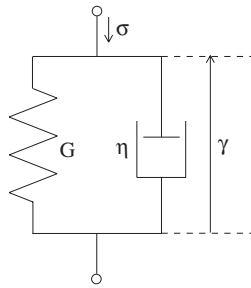


Fig. 17. Voigt model.

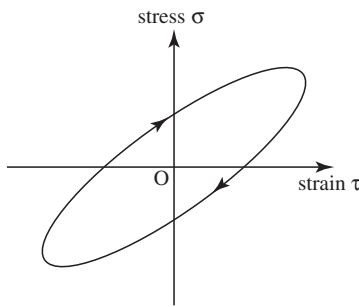


Fig. 18. Illustration of stress–strain diagram of tissue.

$$\sigma = E\gamma + \eta \frac{d\gamma}{dt}, \tag{5.1}$$

where E is Young’s modulus, η is the viscosity coefficient, σ is the stress, and γ is the strain. In this study, prototype ultrasonic knives were driven by harmonic oscillation. Therefore, the stress σ is expressed as follows:

$$\sigma = \sigma_0 \sin \omega t. \tag{5.2}$$

By substituting eq. (5.2) into eq. (5.1), the strain γ can be described by

$$\gamma = \frac{\sigma_0}{E \sqrt{1 + \left(\frac{\eta}{E}\right)^2}} \sin(\omega t - \theta) = \gamma_0 \sin(\omega t - \theta), \tag{5.3}$$

$$\theta = \tan^{-1} \omega \frac{\eta}{E} = \tan^{-1} \omega \tau. \tag{5.4}$$

From eq. (5.3), strain γ has a phase delay θ from stress σ , as shown in eq. (5.4). Therefore, the stress–strain relationship generally shows a hysteresis property, as shown in Fig. 18. The area within the stress–strain diagram W_h corresponds to the evaporated energy per period.

$$W_h = \oint \sigma d\gamma \tag{5.5}$$

The time derivative of eq. (5.3) is shown as follows:

$$\frac{d\gamma}{dt} = \omega \gamma_0 \cos(\omega t - \theta). \tag{5.6}$$

By substituting eqs. (5.2) and (5.6) into eq. (5.5), the evaporated energy W_h per period is given by

$$\begin{aligned} W_h &= \oint \sigma d\gamma \\ &= \int_0^{2\pi/\omega} \omega \sigma_0 \gamma_0 \sin \omega t \cos(\omega t - \theta) dt \end{aligned}$$

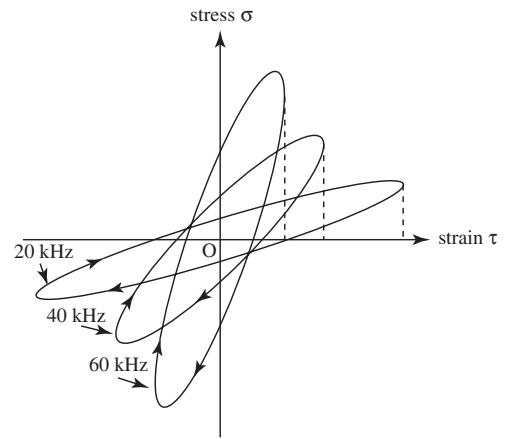


Fig. 19. Stress–strain diagrams at different frequencies.

$$\begin{aligned} &= \frac{1}{2} \omega \sigma_0 \gamma_0 \int_0^{2\pi/\omega} \{\sin(2\omega t - \theta) + \sin \theta\} dt \\ &= \pi \sigma_0 \gamma_0 \sin \theta. \end{aligned} \tag{5.7}$$

As shown by eq. (5.4), phase delay θ is a function of ω , and θ becomes larger as ω increases. Thus, the evaporated energy per period is proportional to the operation frequency ω . In this section, the difference in heat generation is discussed on the basis of the hysteresis property of the stress–strain relationship.

First, the heat generation at the tissue surface is discussed. The stress–strain relationship at different frequencies is illustrated in Fig. 19. According to eq. (5.7), the area of the stress–strain relationship in Fig. 19 depends on stress σ , strain γ , and phase delay θ . The area becomes larger with higher frequency because phase delay θ becomes larger with higher frequency, as shown in eq. (5.4). Moreover, the coagulation of the tissue surface per unit time depends on the vibration frequency because the vibration frequency determines the rotation number of the stress–strain diagram per unit time. As shown in Fig. 10, the coagulated depths are similar for various frequencies when the vibration amplitude is constant. However, even in the case of the same vibration velocity, the vibration amplitude at a lower frequency becomes larger than that at a higher frequency. Thus, the coagulated depth becomes larger with lower frequency, as shown in Fig. 7(b).

Next, the heat generation in the case of applying pressure load is discussed. Figure 20(a) illustrates the nonlinear stress–strain relationship of tissue. Young’s modulus is the gradient of the stress–strain curve shown in Fig. 20(a). When pressure load is applied, the tissue is compressed and becomes hard. That is, Young’s modulus E is increased due to the pressure load and the stress–strain relationship shifts towards the right-hand side, as shown in Fig. 20(b). Thus, the heat generation due to the expansion and contraction of tissue is increased due to the increase in the area of the stress–strain relationship.

Finally, the difference in heat generation depending on the vibration mode is discussed. Viscoelasticity in longitudinal vibration is determined by Young’s modulus E and viscosity coefficient η . On the other hand, it is determined by shear modulus G and shear viscosity coefficient λ in shear vibration. Young’s modulus is equivalent to three times

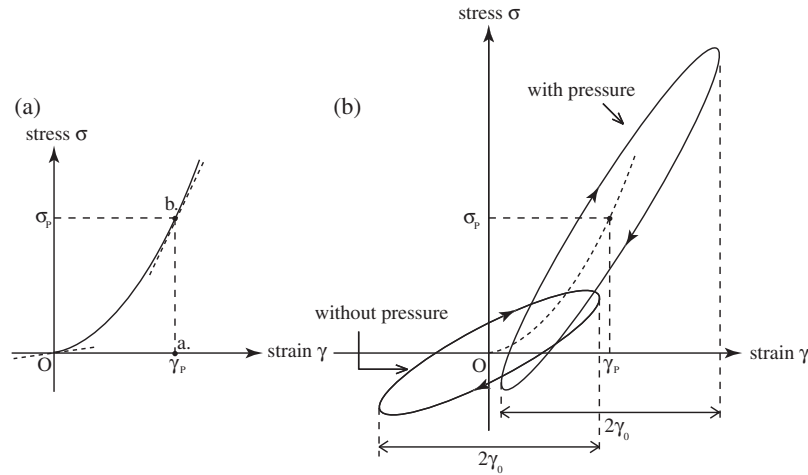


Fig. 20. Illustrations of (a) change in elasticity due to the static pressure and (b) change in hysteresis property due to static pressure.

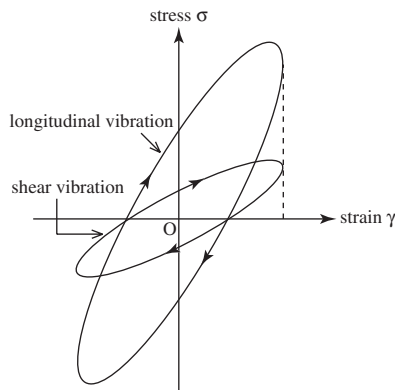


Fig. 21. Illustration of stress–strain diagrams for different vibration modes.

the shear modulus ($E = 3G$); the same is true for the viscosity coefficient ($\eta = 3\lambda$).²²⁾ Figure 21 shows the stress–strain relationship for these two vibration modes when the same amplitude of strain is generated. In Fig. 21, the heat generation caused by shear vibration is smaller than that caused by longitudinal vibration, which corresponds to the difference in Fig. 16.

In this section, we qualitatively discussed heat generation using the stress–strain relationship, because the physical constants or stress used for the calculation of heat generation was unknown. A quantitative discussion of heat generation still remains for future work.

6. Conclusions

In this paper, we focused on the vibration frequency of an ultrasonic surgical knife. Frequency characteristics in the cutting of soft tissue were investigated using prototype knives operated at 24.2, 44.8, and 71.4 kHz. The coagulation ratio and coagulated depth were different for each knife. At a lower frequency, the region of the coagulated tissue was deeper compared with at a higher frequency. At the same time, when the operation frequency was higher, coagulated tissue was distributed in the region closer to the surface compared with that at a lower frequency. The coagulation of tissue along the depth direction depends on the vibration amplitude. The dependence of tissue coagulation on the

pressure load, contact of the tip with tissue, and vibration mode was investigated. These results were discussed in terms of heat generation caused by the stress–strain relationship of soft tissue. The results will be effective in the consideration of frequency characteristics in the cutting of soft tissue using an ultrasonic surgical knife, and also useful for the identification of the optimum operation frequency.

- 1) F. J. Fry and L. K. Johnson: *Ultrasound Med. Biol.* **4** (1978) 337.
- 2) P. Zhong, L. Cioanta, F. H. Cocks, and G. M. Preminger: *J. Acoust. Soc. Am.* **101** (1997) 2940.
- 3) X. Xi and P. Zhong: *Ultrasound Med. Biol.* **26** (2000) 457.
- 4) H. Kanai, Y. S. Jang, N. Chubachi, and Y. Tanahashi: *Jpn. J. Appl. Phys.* **33** (1994) 3159.
- 5) Y. S. Jang, T. Akasaka, M. Sato, H. Kanai, and N. Chubachi: *Jpn. J. Appl. Phys.* **35** (1996) 3163.
- 6) Z. Xu, L. Y. Eun, T. L. Hall, B. C. Tran, J. B. Fowlkes, and C. A. Cain: *IEEE Trans. Ultrason. Ferroelectr. Freq. Control* **51** (2004) 726.
- 7) Z. Xu, J. B. Fowlkes, E. D. Rothman, A. M. Levin, and C. A. Cain: *J. Acoust. Soc. Am.* **117** (2005) 424.
- 8) U. Tsuda, E. Mori, and S. Ueha: *Proc. 3rd Symp. Ultrasonic Electronics, Tokyo, 1982*, *Jpn. J. Appl. Phys.* **22** (1983) Suppl. 22-3, p. 105.
- 9) J. F. Amaral: *Surg. Laparosc. Endosc.* **4** (1994) 92.
- 10) T. F. Molnar, Z. Szantó, T. László, L. Lukacs, and Ö. P. Horvath: *Eur. J. Cardio-thorac. Surg.* **26** (2004) 1192.
- 11) H. Inaba, Y. Kaneko, T. Ohtsuka, M. Ezure, K. Tanaka, K. Ueno, and S. Takamoto: *Soc. Thorac. Surg.* **69** (2000) 1399.
- 12) N. Luciani, A. Anselmi, M. Gaudino, G. Nasso, F. Glieca, L. Martinelli, F. Santarelli, M. Perisano, and G. Possati: *Soc. Thorac. Surg.* **80** (2005) 934.
- 13) C. Cordon, R. Fajardo, J. Ramirez, and M. F. Herrera: *Surgery* **137** (2005) 337.
- 14) J. P. Willging and B. J. Wiatrak: *Otolaryngol. Head Neck Surg.* **128** (2003) 318.
- 15) T. Isomura, H. Suma, T. Sato, and T. Horii: *Eur. J. Cardiothorac. Surg.* **14** (1998) 101.
- 16) W. W. Cimino and L. J. Bond: *Ultrasound Med. Biol.* **22** (1996) 89.
- 17) C. Koch, T. Friedrich, F. Metternich, A. Tannapfel, H. P. Reimann, and U. Eichfeld: *Ultrasound Med. Biol.* **29** (2003) 301.
- 18) C. Koch, M. Borys, T. Fedtke, and U. Richter: *Proc. IEEE Ultrasonics Symp.*, 2001, p. 1393.
- 19) C. Ying, Z. Zhaoying, and Z. Ganghua: *Ultrasound Med. Biol.* **32** (2006) 415.
- 20) Y. Saito, T. Tsuchiya, and N. Endoh: *Jpn. J. Appl. Phys.* **45** (2006) 4693.
- 21) S. Umemura: *Chou-onpa Tekuno* (Ultrasound TECHNO) (Japan Industrial Publishing, Tokyo, 2004), p. 24 [in Japanese].
- 22) T. Nakagawa: *Reoroji* (Rheology) (Iwanami, Tokyo, 1978) 2nd ed., p. 22 [in Japanese].